

Lifshitz Scaling Effects on Holographic Superconductors

Jun-Wang Lu^{1,2}, Ya-Bo Wu^{1,*}, Peng Qian², Yue-Yue Zhao¹, and Xue Zhang¹

¹*Department of Physics, Liaoning Normal University, Dalian, 116029, China*

²*State Key Laboratory of Theoretical Physics, Institute of Theoretical Physics,
Chinese Academy of Sciences, Beijing 100190, China*

Via numerical and analytical methods, the effects of the Lifshitz dynamical exponent z on the holographic superconductor models are studied in some detail, including s-wave and p-wave models. Working in the probe limit, we calculate the condensation and conductivity in both Lifshitz black hole and soliton backgrounds with a general z . For both the s-wave and p-wave models in the black hole backgrounds, as z increases, the phase transition becomes difficult and the conductivity is suppressed. For the Lifshitz soliton backgrounds, when z increases, the critical chemical potential increases in both the s-wave model (with a fixed mass of the scalar field) and p-wave model. For the p-wave model in both the Lifshitz black hole and soliton backgrounds, the anisotropy between the AC conductivity in different spatial directions is suppressed when z increases. In all cases, we find that the critical exponent of the condensation is always one half, independent of z and spacetime dimension. The analytical results from the Sturm-Liouville variational method uphold the numerical calculations. The implications of these results are discussed.

PACS numbers: 11.25.Tq, 04.70.Bw, 74.20.-z

Keywords: AdS/CFT correspondence, Holographic superconductor, Lifshitz gravity

I. INTRODUCTION

The gauge/gravity correspondence provides us a powerful tool to study the strongly coupled field theory via its dual gravity description [1-3]. Over the past years the gauge/gravity duality has been intensively used to study many systems in condensed matter physics. One of interesting applications of the duality is to study high temperature superconductors, which are supposed to be a strongly coupled system. The holographic s-wave superconductor model was first realized via an Einstein-Maxwell theory coupled to a complex scalar field in a Schwarzschild-AdS black hole background [4, 5]. The condensation of the scalar breaks the U(1) symmetry of the system, mimicking the conductor/superconductor phase transition. The authors of [6] analytically studied

*E-mail address:ybwu61@163.com

the superconductor phase transition near the critical point. By a SU(2) gauge field in the bulk, a holographic p-wave superconductor model was constructed in Ref. [7], in which the condensed vector field breaks the U(1) symmetry (one of subgroup of SU(2)) as well as spatial rotational symmetry spontaneously. An alternative holographic p-wave superconductor model is realized by condensation of a 2-form field in a five-dimensional gauged supergravity [8]. The effect of the Gauss-Bonnet term on the p-wave model is discussed in [9, 10]. Very recently a holographic p-wave superconductor model has been constructed in an Einstein-Maxwell-complex vector field theory with a negative cosmological constant [11, 12], where a rich phase structure is found than the SU(2) model. In addition, the holographic d-wave superconductor models are also built by introducing a charged massive spin-two field propagating in the bulk [13–15].

On the other hand, the holographic insulator/superconductor phase transition was studied in a five-dimensional AdS soliton background coupled to a Maxwell field and a charged scalar field [16]. It was shown that when the chemical potential is beyond a critical value μ_c , the pure AdS soliton solution modeling the insulator with a mass gap becomes unstable and results in a new hairy soliton solution dual to a superconducting phase in the boundary field theory. Further studies based on this model can be found, for example, in Refs. [17–23]. Here we stress that those studies are all based on the AdS soliton background. However, for the p wave model in the AdS soliton background, up to now, the conductivity has been calculated only in the direction perpendicular to the condensed vector [21]. To see the anisotropy of the p-wave superconductor model, it is helpful to calculate the conductivity along the condensed vector.

Recently, the phase transitions in many condensed matter systems are found to be governed by the so called Lifshitz fixed points which exhibit the anisotropic scaling of spacetime $t \rightarrow b^z t, \vec{x} \rightarrow b\vec{x}$ ($z \neq 1$), where z is the dynamical critical exponent representing the anisotropy of the spacetime. The gravity description dual to this scaling in the $D = d + 2$ dimensional spacetime was proposed in Ref. [24]

$$ds^2 = L^2 \left(-r^{2z} dt^2 + r^2 d\vec{x}^2 + \frac{dr^2}{r^2} \right), \quad (1)$$

where $d\vec{x}^2 = dx_1^2 + \dots + dx_d^2$ and $r \in (0, \infty)$. This geometry reduces to the AdS spacetime when $z = 1$, while it is a gravity dual with the Lifshitz scaling as $z > 1$. The Lifshitz spacetime (1) can be realized by a massless scalar field coupled to an Abelian gauge field in the following action [25]

$$S = \frac{1}{16\pi G_{d+2}} \int d^{d+2}x \sqrt{-g} \left(R - 2\Lambda - \frac{1}{2} \partial_\mu \varphi \partial^\mu \varphi - \frac{1}{4} e^{b\varphi} \mathcal{F}_{\mu\nu} \mathcal{F}^{\mu\nu} \right). \quad (2)$$

The generalization of (1) to the case with finite temperature is [26]

$$ds^2 = L^2 \left(-r^{2z} f(r) dt^2 + \frac{dr^2}{r^2 f(r)} + r^2 \sum_{i=1}^d dx_i^2 \right), \quad (3)$$

where

$$f(r) = 1 - \frac{r_+^{z+d}}{r^{z+d}}, \quad \Lambda = -\frac{(z+d-1)(z+d)}{2L^2}, \quad (4)$$

$$\mathcal{F}_{rt} = \sqrt{2L^2(z-1)(z+d)r^{z+d-1}}, \quad e^{b\varphi} = r^{-2d}, \quad b^2 = \frac{2d}{z-1}. \quad (5)$$

The Hawking temperature of the Lifshitz black hole is

$$T = \frac{(z+d)r_+^z}{4\pi}, \quad (6)$$

where r_+ denotes the black hole horizon. It is interesting to construct holographic superconductor model by using Lifshitz black hole solutions and to see the effect of the dynamical critical exponent on the properties of holographic superconductors. Indeed some works have been carried out on this topic, see, for example, Refs. [27–31]. In [27] the authors simply studied the scalar condensation in a (3+1)-dimensional Lifshitz black hole background with $z = 3/2$, while Ref. [28] constructed a s-wave superconductor model in a (3+1)-dimensional Lifshitz black hole spacetime with $z = 2$. Bu in [29] studied s-wave and p-wave superconductor models in the (3+1)-dimensional Lifshitz black hole spacetime (3) with $z = 2$. Ref. [30] studied a s-wave model in (3+1)-dimensional hyperscaling violation spacetime with $\theta = 1$ and $z = 2$. Recently, Abdalla et al in [31] have investigated the s-wave superconductor phase transition in a three-dimensional Lifshitz black hole in new massive gravity with $z = 3$ and found a series of peaks in the conductivity for certain values of the frequency.

In this work, we are going to study systematically the effects of the Lifshitz dynamical exponent z on the holographic superconductors based on the Lifshitz spacetime (3) in the probe limit. The holographic models include s-wave and p-wave cases. For all cases, there exists a critical temperature T_c , which decreases when z increases ($z = 1, 2$ in $D = 4$ and $z = 1, 2, 3$ in $D = 5$). This indicates that the increasing z inhibits the superconducting condensation. For the p-wave case, the difference between the AC conductivity in y direction σ_{yy} and in x direction σ_{xx} is suppressed as z increases. We will also study the holographic insulator/superconductor phase transition in the Lifshitz soliton background, which is obtained by double Wick rotation to the Lifshitz black hole spacetime (3). This part is totally new, there does not exist any relevant study in the literature. As z increases, the insulator/superconductor phase transition becomes easy (the critical chemical potential decreases) in the s-wave model (with a fixed operator dimension) but

hard (the critical chemical potential increases) in the p-wave model. In addition, we will study these superconducting phase transition by Sturm-Liouville variational method. The analytical method supports the numerical calculations.

This paper is organized as follows. In section II, we study the s-wave conductor/superconductor and insulator/superconductor phase transitions in the Lifshitz black hole and soliton backgrounds, respectively, by numerical calculations and analytical method. The p-wave conductor/superconductor (insulator/superconductor) phase transitions will be studied in Sec. III. The final section is devoted to the conclusions and discussions.

II. HOLOGRAPHIC S-WAVE SUPERCONDUCTORS IN THE LIFSHITZ SPACETIME

In this section, we first study the holographic s-wave superconductor model in the Lifshitz black hole background. To complement the numerical calculations, we also study the conductor/superconductor phase transition by the Sturm-Liouville variational method. In the second part of this section, we will study the holographic s-wave superconductor model in the Lifshitz soliton background.

Following Ref. [4], we consider the following Lagrangian consisting of a Maxwell field and a complex scalar field

$$L_m = -\frac{1}{4}F_{\mu\nu}F^{\mu\nu} - |D_\mu\psi|^2 - m^2|\psi|^2, \quad (7)$$

where $D_\mu = \nabla_\mu - iqA_\mu$, $F_{\mu\nu} = \nabla_\mu A_\nu - \nabla_\nu A_\mu$ and m (q) is the mass (charge) of the scalar field ψ . From (7) we have the equations of motion of ψ and the Maxwell field

$$D_\mu D^\mu \psi - m^2 \psi = 0, \quad (8)$$

$$\nabla^\mu F_{\mu\nu} - iq(\psi^* D_\nu \psi - \psi D_\nu^* \psi^*) = 0. \quad (9)$$

We will work in the so-called probe approximation, namely the back reaction of the matter sector (7) on the background Lifshitz geometry is neglected. In addition, by using the gauge symmetry in (7), we can consider the following ansatz for the scalar field and Maxwell field as

$$\psi = \psi(r), \quad A_\mu dx^\mu = \phi(r)dt. \quad (10)$$

A. s-wave superconductors in the Lifshitz black hole background

In this subsection we study the holographic s-wave superconductor model in the Lifshitz black hole background (3). In this case, the equations of motion (8) and (9) in the background (3) reduce

to

$$\psi'' + \left(\frac{d+z+1}{r} + \frac{f'}{f} \right) \psi' + \frac{q^2 \phi^2}{r^{2z+2} f^2} \psi - \frac{m^2 L^2}{r^2 f} \psi = 0, \quad (11)$$

$$\phi'' + \frac{d-z+1}{r} \phi' - \frac{2q^2 L^2 \psi^2}{r^2 f} \phi = 0, \quad (12)$$

where a prime stands for the derivative with respect to r . To solve the above equations, we have to specify the boundary conditions for the two fields. At the horizon $r = r_+$, we impose $\phi(r_+) = 0$ to satisfy the finite norm of A_μ , while $\psi(r_+)$ needs to be regular. At the boundary $r \rightarrow \infty$, $\psi(r)$ and $\phi(r)$ behave as

$$\psi(r) = \frac{\psi_1}{r^{\Delta_-}} + \frac{\psi_2}{r^{\Delta_+}} + \dots, \quad (13)$$

$$\phi(r) = \mu - \frac{\rho}{r^{d-z}} + \dots (z < d), \text{ and } \mu - \rho \ln \xi r + \dots (z = d), \quad (14)$$

where $\Delta_\pm = \frac{z+d \pm \sqrt{(z+d)^2 + 4m^2}}{2}$, ξ , ψ_1 , ψ_2 , μ and ρ are all constants. According to the gauge/gravity duality, ψ_1 (ψ_2) can be regarded as the source (the expectation value) of the dual operator \mathcal{O} , and μ and ρ are chemical potential and charge density of dual field theory. Since we require that the U(1) symmetry is broken spontaneously, we impose the source-free condition $\psi_1 = 0$. We denote $\Delta = \Delta_+$ throughout the paper. The mass squared m^2 of the scalar field has a lower bound as $m^2 = -(z+d)^2/4$ with $\Delta = \Delta_{BF} = (z+d)/2$. In that case, there is a logarithmic term in the asymptotical expansion (13). We treat such a term as the source which is set to be zero to avoid the instability induced by this term following [5]. In this paper we consider canonical ensemble where ρ is fixed, when we discuss the black hole backgrounds.

In the numerical calculations, we will set $L = 1$ and $q = 1$ for simplicity. Concretely we focus our numerical calculation on the cases of $z = 1, 2$ in $D = 4$ and $z = 1, 2, 3$ in $D = 5$. To see clearly the effect of the dynamical critical exponent z , we fix the dimension Δ of the boundary scalar operator. Figure 1 shows the condensation as a function of temperature for various z , from which we can see that the condensation decreases with the increase of z . Note that in the $D = 5$ case, the curves of the condensation for $z = 2$ and $z = 3$ intersects at some low temperature. In fact in the numerical calculations, we find that the condensation for the case of $z = 2$ in $D = 4$ and of $z = 3$ in $D = 5$ increase slight quickly at low temperature than other curves. This might be due to the fact that for the cases $z = 2$ in $D = 4$ and $z = 3$ in $D = 5$, there is a logarithmic term in the gauge field ϕ expansion near the boundary $r \rightarrow \infty$. In addition, at the sufficiently low temperature, the back reaction effect of the matter sector on the background geometry becomes important, thus the probe approximation considered in this paper is no longer valid. For a comparison, we list in Tab. I the

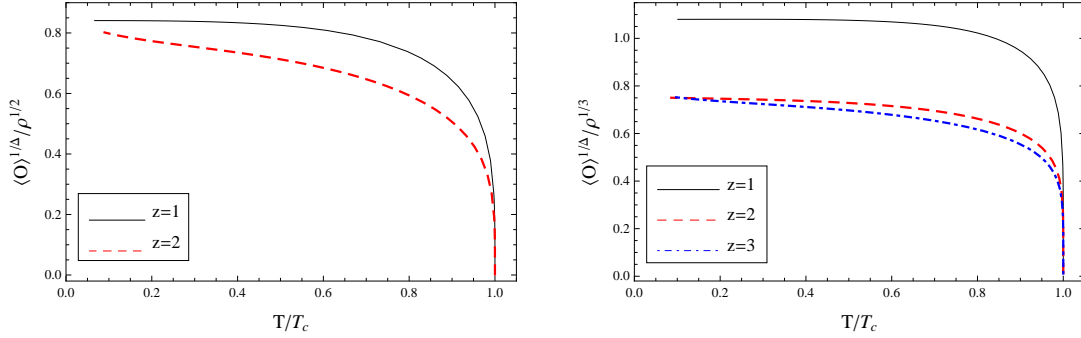


FIG. 1: The condensation versus temperature in the s-wave model for $\Delta = 2$ in $D = 4$ (left) and $\Delta = 3$ in $D = 5$ (right). The curves from top to bottom in the left plot correspond to $z = 1$ (solid), 2 (dashed), while the ones in the right plot to $z = 1$ (solid), 2 (dashed), 3 (dotted), respectively.

critical temperature T_c and the condensation behavior near T_c for the cases of $z = 1, 2$ and 3 with different operator dimension. From the table, we can find that when we increase z , T_c decreases for the case with a fixed Δ , which indicates that the increasing anisotropy between space and time hinders the phase transition. This can be understood as follows. We can see from Eq. (11) that near the horizon, the effective mass of the scalar field increases as the dynamical critical exponent z increases. This leads to a lower critical temperature as z increases. Here we mention that the condensation in the case with $z = 2$, $m^2 = -3$, $D = 4$ is also calculated in Ref. [28], but the latter works in a grand canonical ensemble, while in the cases with $z = 2$, $m^2 = -3$ (0), $D = 4$, our results are consistent with the ones in Ref. [29]. On the other hand, we can see from the Tab. I that all curves of condensation versus temperature have a square root behavior near T_c , which suggests that the critical exponent is $1/2$, as expected from the mean field theory.

To compute the AC conductivity in the boundary field theory side, we need to study the perturbation of the gauge field in the bulk. Due to the rotational symmetry of the s-wave superconductor model, without loss of generality, we turn on the perturbation along the x direction with the ansatz $\delta A_\mu = A_x(r)e^{-i\omega t}$. The linearized equation of the perturbation A_x turns out to be

$$A_x'' + \left(\frac{d+z-1}{r} + \frac{f'}{f} \right) A_x' + \frac{\omega^2}{r^{2z+2} f^2} A_x - \frac{2\psi^2}{r^2 f} A_x = 0. \quad (15)$$

At the horizon, we impose the ingoing wave condition

$$A_x(r) = (r - r_+)^{-i\omega/4\pi T} (1 + A_{x1}(r - r_+) + A_{x2}(r - r_+)^2 + A_{x3}(r - r_+)^3 + \dots). \quad (16)$$

And at the boundary $r \rightarrow \infty$, the asymptotical expansion of $A_x(r)$ is of the form

$$A_x(r) = A^{(0)} + \frac{A^{(d+z-2)}}{r^{d+z-2}} + \dots. \quad (17)$$

TABLE I: The critical temperature, condensation and superfluid density for the s-wave superconductor in the 4(5)-dimensional Lifshitz black hole backgrounds. Here $t = 1 - T/T_c$, the subscript SL denotes the quantity calculated by the Sturm-Liouville method, and $\langle \mathcal{O} \rangle^{1/\Delta} / \rho^{1/d}$ and $n_s / \rho^{(d+z-2)/d}$ as well as $\langle \mathcal{O} \rangle_{SL}^{1/\Delta} / \rho^{1/d}$ are calculated near T_c .

D	z	m^2	Δ	$T_c / \rho^{z/d}$	$\langle \mathcal{O} \rangle^{1/\Delta} / \rho^{1/d}$	$n_s / \rho^{(d+z-2)/d}$	$T_{c;SL} / \rho^{z/d}$	$\langle \mathcal{O} \rangle_{SL}^{1/\Delta} / \rho^{1/d}$
4	1	-2	2	0.118	$1.19t^{1/2\Delta}$	$2.82t$	0.117	$0.95t^{1/2\Delta}$
4	1	-5/4	5/2	0.099	$1.06t^{1/2\Delta}$	$2.43t$	0.097	$0.80t^{1/2\Delta}$
4	2	-4	2	0.068	$0.92t^{1/2\Delta}$	$1.95t$	—	—
4	2	-15/4	5/2	0.047	$0.76t^{1/2\Delta}$	$1.25t$	—	—
4	2	-3	3	0.035	$0.66t^{1/2\Delta}$	$0.88t$	—	—
4	2	0	4	0.023	$0.31t^{1/2\Delta}$	$0.50t$	—	—
5	1	-15/4	5/2	0.220	$1.56t^{1/2\Delta}$	$5.19t$	0.218	$1.36t^{1/2\Delta}$
5	1	-3	3	0.197	$1.44t^{1/2\Delta}$	$4.49t$	0.196	$1.22t^{1/2\Delta}$
5	1	-7/4	7/2	0.182	$1.36t^{1/2\Delta}$	$3.87t$	0.180	$1.10t^{1/2\Delta}$
5	1	0	4	0.171	$1.30t^{1/2\Delta}$	$3.38t$	0.168	$1.01t^{1/2\Delta}$
5	2	-6	3	0.087	$0.90t^{1/2\Delta}$	$1.53t$	0.087	$0.94t^{1/2\Delta}$
5	2	-21/4	7/2	0.074	$0.91t^{1/2\Delta}$	$1.12t$	0.074	$0.85t^{1/2\Delta}$
5	2	-4	4	0.064	$0.76t^{1/2\Delta}$	$0.86t$	0.064	$0.77t^{1/2\Delta}$
5	3	-9	3	0.045	$0.82t^{1/2\Delta}$	$0.93t$	—	—
5	3	-35/4	7/2	0.035	$0.75t^{1/2\Delta}$	$0.57t$	—	—
5	3	-8	4	0.028	$0.68t^{1/2\Delta}$	$0.40t$	—	—

Note that in the case of $z = 1, d = 3$, a logarithmic term $\frac{A^{(0)}\omega^2}{2r^2} \ln \xi r$ should be added to the right hand side of (17), where ξ is a constant. According to the Kubo formula, the AC conductivity reads

$$\sigma(\omega) = \frac{-1}{i\omega} \lim_{r \rightarrow \infty} r^{d+z-1} \frac{A'_x}{A_x}. \quad (18)$$

In the case of $z = 1$ in $d = 3$, a logarithmic divergence exists in $\sigma(\omega)$, which can be canceled by the holographic renormalization [5]. The AC conductivity is plotted in Fig. 2. Here some remarks are in order.

- (1) There exists a pole in the imaginary part in $D = 4$ (5) at zero frequency. This pole corresponds to a delta function in the real part from the Kramers-Kronig relation, which is the signal of DC superconductivity.
- (2) In the case of $z = 1$ in $D = 4$ (5), when the temperature decreases, there exists a sharp gap

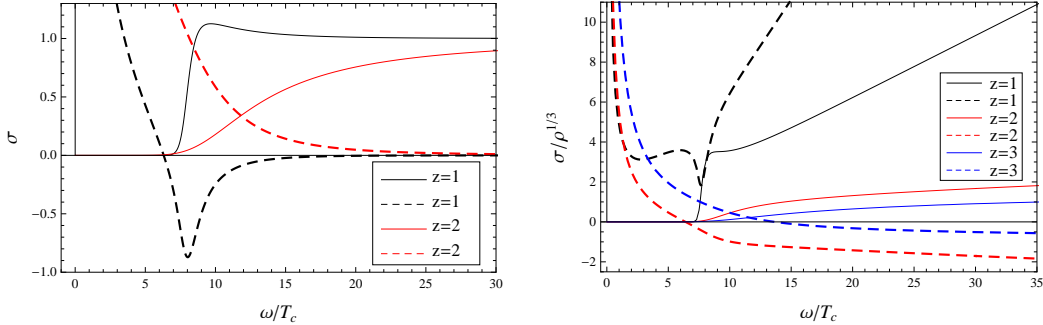


FIG. 2: The real (solid) and imaginary (dashed) part of the AC conductivity versus frequency of the s-wave model at $T/T_c \approx 0.1$ with $\Delta = 2$, $z = 1$ (black), 2 (red) in $D = 4$ (left), and $\Delta = 3$, $z = 1$ (black), 2 (red), 3 (blue) in $D = 5$ (right).

frequency ω_g . The ratio $\omega_g/T_c \approx 8$, much larger than the weak coupling BCS theory value 3.5, indicates that the holographic model indeed describes a strongly coupled field theory. In addition, we can clearly see from Fig. 2 that when $z \neq 1$ in $D = 4$ and $D = 5$, the minimum of the imaginary part of the conductivity disappears, which means that in those cases, the energy gap is no longer obvious.

- (3) In the case of $D = 4$, we see from the left plot of Fig. 2 that the real part of the conductivity is suppressed in the case of $z = 2$, compared to the case of $z = 1$. The same happens in the case of $D = 5$, the conductivity for the case $z > 1$ is suppressed. This shows the anisotropic effect of the background spacetime.
- (4) In the $z = 1$ and $D = 5$ case, both the real and imaginary parts of the conductivity diverge as $w \rightarrow \infty$, which is quite different from the corresponding case in $D = 4$ dimensions. This behavior disappears when $z > 1$. This is due to the absence of the logarithmic term in the expansion of A_x near the boundary $r \rightarrow \infty$.

The superfluid density n_s can be calculated as the coefficient of the pole in $Im[\sigma]$ at $\omega = 0$, i.e., $n_s \approx \lim_{\omega \rightarrow 0} \omega Im[\sigma]$. In the left plot of Fig. 3, we show n_s with different z with a fixed $\Delta = 3$ in $D = 5$ and we list n_s near T_c in Tab. I for all cases we calculated. We see that in all cases, n_s has the behavior $n_s \sim (1 - T/T_c)$ near the critical point. From the plot we see n_s decreases with the increase of z . This is consistent with the result that the conductivity decreases as z increases, shown in Fig. 2.

Next we turn to the analytical study on the critical behavior of the s-wave superconductor model by employing the Sturm-Liouville variational method [6]. Due to the presence of the logarithmic term in the falloff of the gauge field ϕ for the case of $z = d$, it is difficult to expand ϕ near the

boundary. To avoid this, we here consider the case of $1 \leq z < d$. Taking the new variable $u = r_+/r$, Eqs. (11) and (12) can be rewritten as

$$\psi'' + \frac{u^{d+z} + d + z - 1}{u(u^{d+z} - 1)}\psi' + \frac{m^2(u^{d+z} - 1) + r_+^{-2z}u^{2z}\phi^2}{u^2(u^{d+z} - 1)^2}\psi = 0, \quad (19)$$

$$\phi'' + \frac{z - d + 1}{u}\phi' + \frac{2\psi^2}{u^2(u^{d+z} - 1)}\phi = 0, \quad (20)$$

where a prime represents the derivative with respect to u . As $T \rightarrow T_c$, the scalar field vanishes, so the solution of $\phi(u)$ is given by

$$\phi(u) = \lambda r_{+c}^z (1 - u^{d-z}), \lambda = \frac{\rho}{r_{+c}^d}, \quad (21)$$

where we have considered $\phi(1) = 0$. We define a new function $F(u)$ as

$$\psi(u) = \frac{\langle \mathcal{O} \rangle}{r_{+c}^\Delta} u^\Delta F(u). \quad (22)$$

We focus on the case of $D = 5$. Substituting Eqs. (21) and (22) into (19), the latter can be rewritten as a Sturm-Liouville eigenvalue equation

$$\frac{d}{du}(\mathcal{T}F') - \mathcal{P}F + \lambda^2 \mathcal{Q}F = 0, \quad (23)$$

where \mathcal{T} , \mathcal{P} , and \mathcal{Q} read

$$\begin{aligned} \mathcal{T} &= (1 - u^{z+3}) u^{\sqrt{4m^2 + z^2 + 6z + 9} + 1}, \\ \mathcal{P} &= \frac{1}{2} \left((z + 3) \left(\sqrt{4m^2 + (z + 3)^2} + z + 3 \right) + 2m^2 \right) u^{\sqrt{4m^2 + (z + 3)^2} + z + 2}, \\ \mathcal{Q} &= -\frac{u^{2z} (u^3 - u^z)^2 u^{\sqrt{4m^2 + (z + 3)^2} - 2z - 1}}{u^{z+3} - 1}. \end{aligned} \quad (24)$$

According to the boundary conditions for $F(u)$, i.e., $F(0) = 1$ and $F'(0) = 0$, we can introduce a trial function

$$F = F_\alpha(u) \equiv 1 - \alpha u^2. \quad (25)$$

The minimal eigenvalue λ^2 is obtained by minimizing the following expression with respect to the coefficient α

$$\lambda^2 = \frac{\int_0^1 du (\mathcal{T}F'^2 - \mathcal{P}F^2)}{\int_0^1 du \mathcal{Q}F^2}. \quad (26)$$

From the minimal eigenvalue of λ^2 , we can read off the dependence of the critical temperature on the parameters m^2 and z . We show the analytical result on the critical temperature versus z and

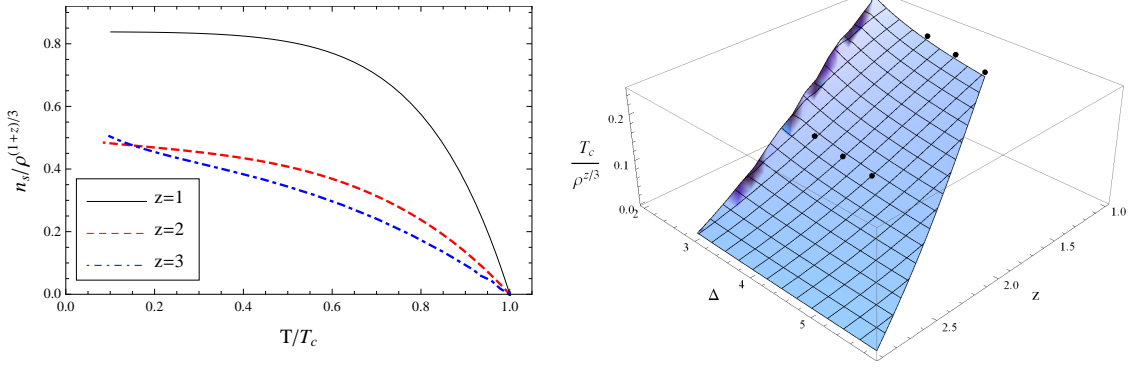


FIG. 3: The superfluid density versus temperature (left) with $\Delta = 3$, $z = 1, 2, 3$ (from top to bottom) and the critical temperature T_c versus z and m^2 (right) of the s-wave model in the 5-dimensional black hole background. The black dots in the right plot are from the numerical calculations with $z = 1, 2$ for $\Delta = 3, 7/2, 4$, respectively.

Δ in the right plot of Fig. 3. From the figure, we find the critical temperature decreases obviously when one increases z , while it decreases gradually with the increasing dimension of operator Δ . Clearly the analytical result is consistent with the numerical one obtained above. In Tab. I we list some critical temperatures $T_{c,SL}$ from the Sturm-Liouville variational method, to compare with the numerical results.

When the temperature is slightly below T_c , the condensation $\frac{\langle \mathcal{O} \rangle^2}{r_+^{2\Delta}}$ is very small. In that case we can expand $\phi(u)$ in the form

$$\frac{\phi(u)}{r_+^z} = \lambda(1 - u^{3-z}) + \frac{\langle \mathcal{O} \rangle^2}{r_+^{2\Delta}} \chi(u) + \dots \quad (27)$$

The equation of $\chi(u)$ reads

$$\chi'' + \frac{z-2}{u} \chi' - \frac{2\lambda(\alpha u^2 - 1)^2 (u^3 - u^z) u \sqrt{4m^2 + (z+3)^2 + 1}}{u^{z+3} - 1} = 0. \quad (28)$$

Considering conditions $\chi(1) = 0$ and $\chi'(1) = 0$, we can have

$$u^{z-2} \chi(u)|_{u \rightarrow 0} = 2\lambda \int_1^0 du \frac{(\alpha u^2 - 1)^2 (u^3 - u^z) u \sqrt{4m^2 + (z+3)^2 + z - 1}}{u^{z+3} - 1}. \quad (29)$$

Next expanding $\chi(u)$ near the boundary $u \rightarrow 0$, $\chi(u) = \chi(0) + \chi'(0)u + \dots$, we obtain

$$\frac{\rho}{r_+^3 \lambda} - 1 = -\frac{\langle \mathcal{O} \rangle^2}{r_+^{2\Delta}} \frac{\chi^{3-z}(0)}{\lambda(3-z)!}, \quad (30)$$

by comparing the coefficient of u^{3-z} in both sides of Eq. (27), where we have used Eq. (14) and Eq. (29). Note that here z is limited to be an integer, $z = 1$ or 2 . Combining $r_{+c} = (\rho/\lambda)^{1/3}$ with the temperature (6), we obtain

$$\langle \mathcal{O} \rangle^{\frac{1}{\Delta}} = \left(\frac{4\pi T_c}{3+z} \right)^{\frac{1}{z}} \left(\frac{\lambda(3-z)!}{-\chi^{(3-z)}(0)} \right)^{\frac{1}{2\Delta}} \left(1 - \left(\frac{T}{T_c} \right)^{\frac{3}{z}} \right)^{\frac{1}{2\Delta}}. \quad (31)$$

We list the condensation in Tab. I, in order to compare with the numerical calculation. We see indeed that the analytical calculation agrees with the numerical one at the same order. It might be worth stressing here that the critical behavior of the condensation $\langle \mathcal{O} \rangle \sim (1 - (T/T_c)^{d/z})^{1/2}$ looks a little different from the standard form $\sim (1 - T/T_c)^{1/2}$. This is due to the scaling symmetry in the Lifshitz spacetime: $r \rightarrow \lambda r, T \rightarrow \lambda^z T, \langle \mathcal{O} \rangle \rightarrow \lambda^\Delta \langle \mathcal{O} \rangle, \rho \rightarrow \lambda^d \rho$. Further expanding (31) near the critical temperature, it is easy to see that the critical exponent is still 1/2 and Eq. (31) can be expressed as

$$\langle \mathcal{O} \rangle^{\frac{1}{\Delta}} = \left(\frac{3}{z}\right)^{\frac{1}{2\Delta}} \left(\frac{4\pi T_c}{3+z}\right)^{\frac{1}{z}} \left(\frac{\lambda(3-z)!}{-\chi^{(3-z)}(0)}\right)^{\frac{1}{2\Delta}} \left(1 - \frac{T}{T_c}\right)^{\frac{1}{2\Delta}}. \quad (32)$$

B. s-wave superconductors in the Lifshitz soliton background

In this subsection we consider the insulator/superconductor phase transition by generalizing the study in the AdS soliton background [16] to the Lifshitz soliton background with general z . By performing the double Wick rotation to the Lifshitz black hole solution (3), a $(d+2)$ dimensional Lifshitz soliton can be obtained as

$$ds^2 = L^2 \left(-r^2 dt^2 + \frac{dr^2}{r^2 f(r)} + r^2 \sum_{i=1}^{d-1} dx_i^2 + r^{2z} f(r) d\chi^2 \right), \quad (33)$$

where $f(r)$ still takes the form (4). To distinguish the soliton from the black hole, we denote the tip of the soliton geometry by r_0 . To avoid a potential conical singularity at the tip, a periodicity on the spatial direction χ has to be imposed with a period $\chi \sim \chi + \frac{4\pi}{(z+d)r_0^z}$. For the soliton solution, there is no horizon, thus temperature is vanishing. Due to the existence of the tip, there is an IR cutoff (mass gap) for the dual field theory. In other words, the dual field theory is in a confined phase. Thus similar to the case of the AdS soliton spacetime, the Lifshitz soliton solution can describe an insulator [16]. In addition, let us notice that because of the compactness of the spatial direction χ , this $(d+2)$ -dimensional soliton geometry is dual to a d dimensional field theory with mass gap, according to the gauge/gravity duality. In particular, we stress here that the Lifshitz soliton background (33) does no longer have the anisotropic scaling $t \rightarrow b^z t$ and $\vec{x} \rightarrow b\vec{x}$ in the boundary spacetime as in the Lifshitz black hole background (3), but the dual boundary spacetime is of only the spatial anisotropy: $t \rightarrow bt$, $\vec{x} \rightarrow b\vec{x}$ and $\chi \rightarrow b^z \chi$.

Now we consider a holographic s-wave superconductor model based on the Lifshitz soliton background (33). The starting point of the matter sector is still the action (7). Due to the symmetry of the background, in the probe approximation, the ansatz for the matter sector is

$A_t = \phi(r)$ and $\psi = \psi(r)$ following Ref. [16]. In the background (33), the equations of motion for ψ and ϕ read

$$\psi'' + \left(\frac{d+z+1}{r} + \frac{f'}{f} \right) \psi' + \frac{q^2 \phi^2}{r^4 f} \psi - \frac{m^2 L^2}{r^2 f} \psi = 0, \quad (34)$$

$$\phi'' + \left(\frac{d+z-1}{r} + \frac{f'}{f} \right) \phi' - \frac{2q^2 L^2 \psi^2}{r^2 f} \phi = 0, \quad (35)$$

Interestingly, we see from the reduced equations of motion that the effective dimension of the spacetime increases from $(d+2)$ to $(d+z+2)$. In other words, the equations of motion (34) and (35) in the $(d+2)$ -dimensional Lifshitz soliton background (33) with dynamical critical exponent z are exactly the same as those in a $(d+z+2)$ -dimensional AdS soliton background. To solve the above two equations, we impose the Neumann-like boundary condition [16] to make both $\psi(r_0)$ and $\phi(r_0)$ finite at the tip $r = r_0$. Near the boundary $r \rightarrow \infty$, $\psi(r)$ obeys the form (13), while $\phi(r)$ is

$$\phi(r) = \mu - \frac{\rho}{r^{d+z-2}} + \dots, \quad (36)$$

where the coefficients μ and ρ are interpreted as the chemical potential and the charge density in the boundary field theory, respectively. We still take $r_0 = 1$, $L = 1$ and $q = 1$ in the numerical calculation. Thus the period of the spatial coordinate χ is $\Gamma = 4\pi/(z+d)$. To compare the effects of z on the holographic superconductors, we rescale the period of χ to π .

From Eqs. (34) and (35), we see that this set of equations are determined by the parameters $(d+z)$ and m^2 . Thus the case of $z = 1$ in $D = 5$ is the same with the case of $z = 2$ in $D = 4$ if the mass of the scalar field is fixed. In Fig. 4, we plot the condensation and charge density ρ versus chemical potential in the case with $z = 1, 2, 3$ and $\Delta = 3$. We can see from the figure that when one fixes the dimension of the operator, the critical chemical potential decreases as z increases. Near the critical point, we have $\langle \mathcal{O} \rangle \sim \sqrt{\mu - \mu_c}$ and $\rho \sim (\mu - \mu_c)$. This means that the critical exponent of the condensation is still $1/2$, while the one for the charge density is one in all cases. This shows the universality of these critical exponents. In Tab. II we list the critical chemical potential μ_c , condensation, and superfluid density in $D = 4$ and $D = 5$ for different mass of the scalar field, for a clear comparison.

To calculate the conductivity, we turn on the perturbation $\delta A = A_x(r)e^{-i\omega t}$, which obeys the following equation

$$A_x'' + \left(\frac{d+z-1}{r} + \frac{f'}{f} \right) A_x' + \frac{\omega^2}{r^4 f} A_x - \frac{2\psi^2}{r^2 f} A_x = 0. \quad (37)$$

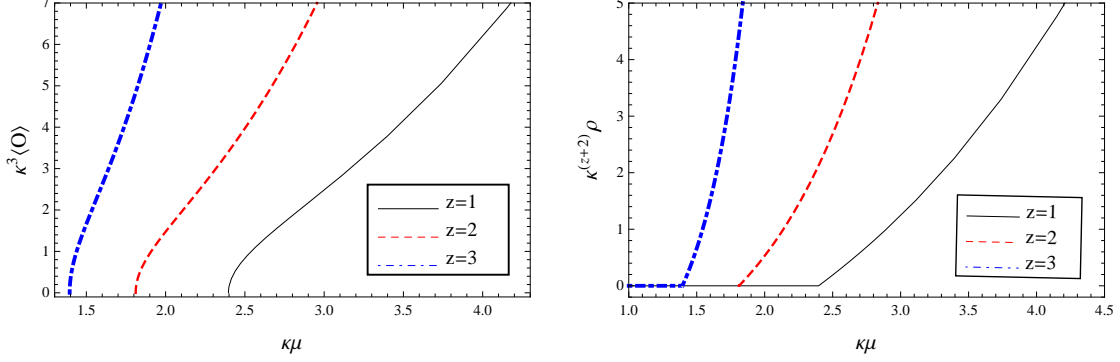


FIG. 4: The condensation (left) and the charge density (right) versus chemical potential of the s-wave superconductor with $\Delta = 3$ and $z = 1, 2, 3$ (from right to left) in the 5-dimensional Lifshitz soliton background, here $\kappa = (4/(3+z))^{1/z}$.

In order for A_x to be finite at the tip, we take the ansatz of A_x near the tip

$$A_x(r) = 1 + A_{s1}(r - r_0) + A_{s2}(r - r_0)^2 + A_{s3}(r - r_0)^3 + \dots \quad (38)$$

where A_{s1} , A_{s2} and A_{s3} are all constants and the leading term is taken to be unity due to the linearity of the equation for A_x . Near the boundary $r \rightarrow \infty$, the general falloff of A_x behaves as

$$A_x(r) = \begin{cases} A^{(0)} + \frac{A^{(1)}}{r} + \dots, & z = 1, d = 2, \\ A^{(0)} + \frac{A^{(2)}}{r^2} + \frac{A^{(0)}\omega^2}{2r^2} \ln \xi r + \dots, & z = 2 (1), d = 2 (3), \\ A^{(0)} + \frac{A^{(0)}\omega^2}{2r^2} + \frac{A^{(3)}}{r^3} + \dots, & z = 3 (2), d = 2 (3), \\ A^{(0)} + \frac{A^{(0)}\omega^2}{4r^2} + \frac{A^{(4)}}{r^4} + \frac{A^{(0)}\omega^4}{16r^4} \ln \xi r + \dots, & z = 3, d = 3, \end{cases} \quad (39)$$

where $A^{(i)}$, and ξ are all constants. Using (18), we calculate the conductivity. Note that when the logarithmic term appears in the expansion (39), its effect on the conductivity can be removed by the holographic renormalization [5], as in the previous subsection. We plot the imaginary part of the conductivity in the case of $D = 5$ in the left plot of Fig. 5. The second pole positions in the imaginary part of the conductivity move toward the right as z increases, which means that the energy of the quasiparticle excitation increases as we increase z . The behavior of the conductivity in the $D = 4$ case is similar as the one in the case of $D = 5$. In Tab. II we list the critical chemical potential, condensation, charge density and superfluid density in $D = 4$ and $D = 5$. We can see that the superfluid density n_s increases when z increases, in the case with a fixed dimension Δ of the scalar operator. This indicates that in this case as z increases the phase transition become easy. This is consistent with the observation that as z increases the critical chemical potential decreases.

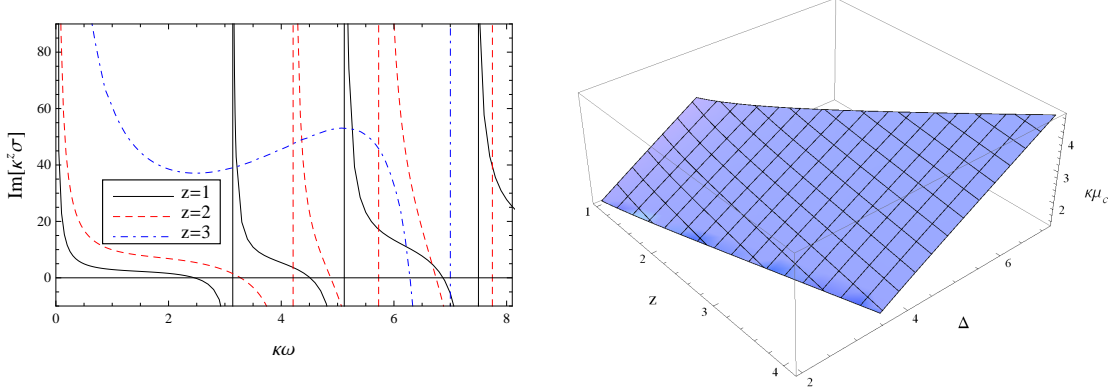


FIG. 5: The conductivity versus frequency with $\Delta = 3$ and $z = 1, 2, 3$ (from bottom to top in the most left) at $\mu/\mu_c \approx 1.74$ (left) and the critical chemical potential μ_c (from the analytical calculation) as a function of Δ and z (right) of the s-wave model in the 5-dimensional Lifshitz soliton background, here $\kappa = (4/(3+z))^{1/z}$.

TABLE II: The numerical and analytical results of the s-wave superconductors in the 4(5)-dimensional Lifshitz soliton backgrounds. Here $t = (\mu/\mu_c - 1)^{1/2}$, $\kappa = (4/(d+z))^{1/z}$, and the subscript SL denotes the quantity calculated by the Sturm-Liouville variational method.

D	z	m^2	Δ	$\kappa\mu_c$	$\kappa^\Delta \langle \mathcal{O} \rangle$	$\kappa^{d+z-1} \rho$	$\kappa^{d+z-2} n_s$	$\kappa\mu_{c;SL}$	$\kappa^\Delta \langle \mathcal{O} \rangle_{SL}$	$\kappa^{d+z-1} \rho_{SL}$
4	1	-2	2	2.291	$3.06t$	$4.34t^2$	$1.89t^2$	2.292	$1.65t$	$2.41t^2$
4	1	-5/4	5/2	2.961	$4.08t$	$4.91t^2$	$1.65t^2$	2.961	$1.89t$	$2.81t^2$
4	1	0	3	3.629	$5.32t$	$5.47t^2$	$1.50t^2$	3.629	$2.11t$	$3.23t^2$
4	2	-15/4	5/2	1.888	$3.41t$	$4.23t^2$	$4.46t^2$	1.890	$2.47t$	$2.51t^2$
4	2	-3	3	2.396	$3.87t$	$4.31t^2$	$3.59t^2$	2.399	$2.82t$	$2.76t^2$
4	3	-25/4	5/2	1.390	$4.29t$	$6.16t^2$	$13.75t^2$	1.392	$3.07t$	$3.16t^2$
4	3	-6	3	1.880	$4.64t$	$5.79t^2$	$8.40t^2$	1.884	$3.54t$	$3.22t^2$
4	3	-21/4	7/2	2.358	$4.87t$	$5.54t^2$	$6.33t^2$	2.363	$4.03t$	$3.36t^2$
5	1	-15/4	5/2	1.888	$3.39t$	$4.23t^2$	$8.48t^2$	1.890	$2.47t$	$2.51t^2$
5	1	-3	3	2.396	$3.85t$	$4.72t^2$	$3.56t^2$	2.398	$2.82t$	$2.76t^2$
5	1	-7/4	7/2	2.901	$4.39t$	$4.55t^2$	$3.08t^2$	2.903	$3.17t$	$2.99t^2$
5	1	0	4	3.404	$4.98t$	$4.70t^2$	$2.75t^2$	3.407	$3.53t$	$3.24t^2$
5	2	-6	3	1.811	$4.06t$	$4.57t^2$	$7.51t^2$	1.815	$3.48t$	$3.10t^2$
5	2	-21/4	7/2	2.272	$4.28t$	$4.29t^2$	$5.66t^2$	2.276	$3.95t$	$3.23t^2$
5	2	-4	4	2.728	$4.58t$	$4.23t^2$	$4.63t^2$	2.732	$4.43t$	$3.39t^2$
5	3	-9	3	1.395	$5.37t$	$7.64t^2$	$21.34t^2$	1.400	$4.13t$	$4.21t^2$
5	3	-35/4	7/2	1.867	$5.36t$	$5.86t^2$	$12.74t^2$	1.872	$4.72t$	$4.08t^2$
5	3	-8	4	2.324	$5.55t$	$3.42t^2$	$10.18t^2$	2.348	$5.35t$	$4.13t^2$

Now, we turn to the analytical calculation of the s-wave model in the 5-dimensional Lifshitz soliton background. In the normal phase, the general solution $\phi(r)$ of Eq. (35) is

$$\phi(u) = C_1 \left(\frac{1}{2u^2} - \frac{{}_2F_1 \left(1, -\frac{2}{d+z}; 1 - \frac{2}{d+z}; u^{d+z} \right)}{2u^2} \right) + C_2, \quad (40)$$

where C_1 and C_2 are two constants, ${}_2F_1$ is the hypergeometric function and $u = r_0/r$. To have a regularity at the tip, we take $C_1 = 0$ as in Refs. [16, 19, 20]. Thus $C_2 = \mu$ giving the chemical potential in the dual field theory. When μ is slightly beyond μ_c , the condensation appears, the scalar field can be expressed as $\psi \approx \langle \mathcal{O} \rangle u^\Delta F(u)$, and the function F obeys the eigenvalue equation

$$\frac{d}{du}(\mathcal{T}F') - \mathcal{P}F + \mu_c^2 \mathcal{Q}F = 0, \quad (41)$$

where \mathcal{T} , \mathcal{P} and \mathcal{Q} are given by

$$\begin{aligned} \mathcal{T} &= (1 - u^{d+z}) u^{\sqrt{(d+z)^2 + 4m^2} + 1}, \\ \mathcal{P} &= \frac{1}{2} \left((d+z)^2 + (d+z) \sqrt{(d+z)^2 + 4m^2} + 2m^2 \right) u^{\sqrt{(d+z)^2 + 4m^2} + d+z-1}, \\ \mathcal{Q} &= u^{\sqrt{(d+z)^2 + 4m^2} + 1}. \end{aligned} \quad (42)$$

By taking the trial function (25), the eigenvalue of μ_c^2 is determined by minimizing the expression (26). We show the critical chemical potential μ_c versus Δ and z in the case of $D = 5$ in the right plot of Fig. 5. We also calculate some cases in $D = 4$ and $D = 5$ as shown in Tab. II. It can be seen that μ_c decreases with the increasing z , but it increases with the operator dimension Δ . This supports our numerical calculations.

In the superconducting phase, near the critical point, the condensation $\langle \mathcal{O} \rangle^2$ is small, so we can expand $\phi(u)$ as

$$\phi(u) = \mu_c + \langle \mathcal{O} \rangle^2 \chi(u) + \dots \quad (43)$$

Note that the approximation $\psi \approx \langle \mathcal{O} \rangle u^\Delta F(u)$, we have the equation of $\chi(u)$ as

$$\chi'' + \frac{(3u^{d+z} + d + z - 3)}{u(u^{d+z} - 1)} \chi' + \frac{2\mu_c (\alpha u^2 - 1)^2 u^{\sqrt{(d+z)^2 + 4m^2} + d+z-2}}{u^{d+z} - 1} = 0. \quad (44)$$

Defining $T(u) = u^{-d-z+3} (1 - u^{d+z})$, Eq. (44) can be rewritten as

$$(T\chi')' - 2\mu_c (\alpha u^2 - 1)^2 u^{\sqrt{(d+z)^2 + 4m^2} + 1} = 0. \quad (45)$$

From the above equation, we can obtain

$$\chi(0) = 2\mu_c \int_1^0 \frac{dy}{T(y)} \int_1^y du (\alpha u^2 - 1)^2 u^{\sqrt{(d+z)^2 + 4m^2} + 1}, \quad (46)$$

$$\chi^{(d+z-2)}(0) = 2\mu_c (d+z-3)! \int_1^0 du (\alpha u^2 - 1)^2 u^{\sqrt{(d+z)^2 + 4m^2} + 1}. \quad (47)$$

Further, near the boundary $u \rightarrow 0$, $\phi(u)$ can be further expanded as [19]

$$\phi(u) = \mu_c + \langle \mathcal{O} \rangle^2 \left(\chi(0) + \chi'(0)u + \frac{1}{2}\chi''(0)u^2 + \frac{1}{6}\chi'''(0)u^3 + \dots \right). \quad (48)$$

Comparing the right hand side of Eq. (48) with $\phi(u) = \mu - \rho u^{d+z-2}$, we obtain

$$\langle \mathcal{O} \rangle = \frac{1}{\sqrt{\chi(0)}} \sqrt{\mu - \mu_c}, \quad (49)$$

$$\rho = \frac{\chi^{(d+z-2)}(0)}{(d+z-2)!\chi(0)} (\mu - \mu_c), \quad (50)$$

where we have used $\chi(1) = 0$ as in Refs. [19, 20] and limited z to be integer. The condensation and the charge density from the analytical method are listed in Tab. II, which matches the numerical calculations at the same order. When $m^2 = -15/4$ and $z = 1$ in $D = 5$, the corresponding results recover the ones in Refs. [16, 19].

III. HOLOGRAPHIC P-WAVE SUPERCONDUCTORS IN LIFSHITZ SPACETIME

In this section, we first study the p-wave superconductor in the Lifshitz black hole by numerical and analytical methods and then discuss the p-wave model in the Lifshitz soliton background. Following the proposals [7], we construct the holographic p-wave superconductor model by considering a SU(2) gauge field in the bulk

$$L_m = -\frac{1}{4} F_{\mu\nu}^a F^{a\mu\nu}, \quad (51)$$

where $F_{\mu\nu}^a$ is the field strength of the gauge field. The SU(2) group has three generators τ^i which satisfy the commutation relation $[\tau^i, \tau^j] = \epsilon^{ijk} \tau^k$ ($i, j = 1, 2, 3$). The equation of motion of the gauge field reads

$$\nabla_\mu F^{a\mu\nu} + \epsilon^{abc} A_\mu^b F^{c\mu\nu} = 0. \quad (52)$$

In this model, a U(1) subgroup generated by τ^3 is treated as the gauge group of electromagnetism, and the gauge boson generated by τ^1 charged by this U(1) is regarded as the vector field. The ansatz is [7]

$$A = \phi(r)\tau^3 dt + \psi(r)\tau^1 dx. \quad (53)$$

When $\psi \neq 0$, according to the gauge/gravity dictionary, the sub-leading term of this field at the boundary gives the expectation value of dual operator J_x , The emergence of the non-trivial vector “hair” breaks the U(1) symmetry and the rotational symmetry, which mimics a p-wave superconducting phase transition in condensed matter physics.

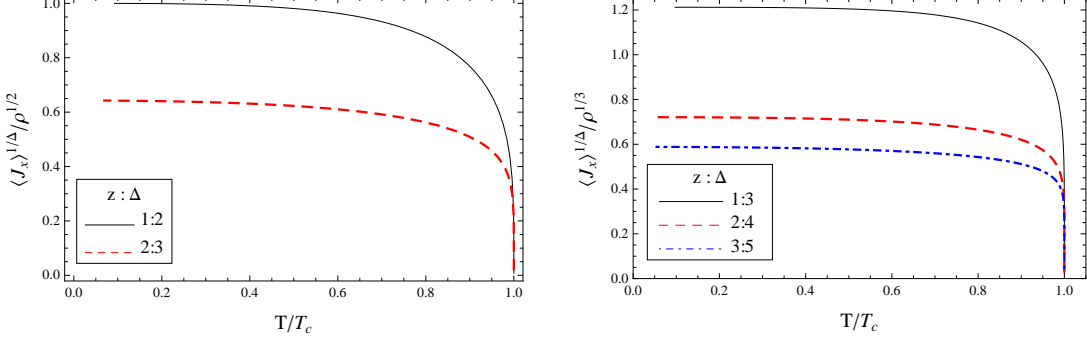


FIG. 6: The condensation versus temperature for the p-wave model in $D = 4$ (left) and $D = 5$ (right) Lifshitz black hole backgrounds.

A. p-wave superconductors in the Lifshitz black hole background

As in the s-wave case, we work in the probe approximation. In that case, the equations of motion of $\phi(r)$ and $\psi(r)$ in the Lifshitz black hole background (3) read

$$\psi'' + \left(\frac{d+z-1}{r} + \frac{f'}{f} \right) \psi' + \frac{\phi^2}{r^{2z+2} f^2} \psi = 0, \quad (54)$$

$$\phi'' + \frac{d-z+1}{r} \phi' - \frac{\psi^2}{r^4 f} \phi = 0. \quad (55)$$

For convenience in numerical calculations, we limit our consideration to the cases $1 \leq z \leq d$ in $D = d + 2 = 4$ and 5 dimensions. At the black hole horizon, we require $\psi(r_+)$ to be regular and $\phi(r_+) = 0$. Near the boundary $r \rightarrow \infty$, $\psi(r)$ behaves as

$$\psi(r) = \psi_0 + \frac{\langle J_x \rangle}{r^{d+z-2}} + \dots, \quad (56)$$

while $\phi(r)$ takes the form (14). We take $\psi_0 = 0$ since ψ_0 is regarded as the source term and the U(1) symmetry is required to be broken spontaneously, while $\langle J_x \rangle$ is viewed as the vacuum expectation value of the vector operator with dimension $\Delta = d + z - 1$ in the boundary field theory.

We plot the condensation behavior in Fig. 6 and list some related results in Tab. IV. We can see from the figure and the table that when z increases, the critical temperature T_c decreases, which implies that the increasing z inhibits the phase transition. For a fixed temperature, the condensation decreases as z increases, this means that the superconductivity becomes weak when we increase z . For all cases, near the critical point, the condensation behaves as $\langle J_x \rangle \sim (1 - T/T_c)^{1/2}$. Once again, it shows the universality of the critical exponent.

The condensation of the vector field happens along the x direction, so the conductivity σ_{xx} along the x direction is expected to be different from that σ_{yy} along the y direction. To calculate

TABLE III: The asymptotical expansion of the perturbation of the p-wave model in the Lifshitz black hole background, where $i = 1, 2$, $\mu = x, y$ and ξ is a constant.

	$d = 3, z = 1$	$d = 3, z = 2$	$d = 3, z = 3$	$d = 2, z = 1$	$d = 2, z = 2$
$a_t^i(r)$	$a_t^{i(0)} + \frac{a_t^{i(2)}}{r^2}$	$a_t^{i(0)} + \frac{a_t^{i(1)}}{r}$	$a_t^{i(0)} + a_t^{i(1)} \ln \xi r$	$a_t^{i(0)} + \frac{a_t^{i(1)}}{r}$	$a_t^{i(0)} + a_t^{i(1)} \ln \xi r$
$a_\mu^3(r)$	$a_\mu^{3(0)} + \frac{a_\mu^{3(2)}}{r^2} + \frac{a_\mu^{3(0)} \omega^2}{2r^2} \ln \xi r$	$a_\mu^{3(0)} + \frac{a_\mu^{3(3)}}{r^3}$	$a_\mu^{3(0)} + \frac{a_\mu^{3(4)}}{r^4}$	$a_\mu^{3(0)} + \frac{a_\mu^{3(1)}}{r}$	$a_\mu^{3(0)} + \frac{a_\mu^{3(2)}}{r^2}$

the conductivity, we turn on the perturbation [7]

$$\delta A = e^{-i\omega t} (a_t^1 \tau^1 dt + a_t^2 \tau^2 dt + a_x^3 \tau^3 dx + a_y^3 \tau^3 dy). \quad (57)$$

The linearized equations of motion of the Yang-Mills field result in four second order equations

$$a_y^{3''} + \left(\frac{d+z-1}{r} + \frac{f'}{f} \right) a_y^{3'} + \frac{\omega^2}{r^{2z+2} f^2} a_y^3 - \frac{\psi^2}{r^4 f} a_y^3 = 0, \quad (58)$$

$$a_t^{1''} + \frac{d-z+1}{r} a_t^{1'} + \frac{\psi \phi}{r^4 f} a_x^3 = 0,$$

$$a_t^{2''} + \frac{d-z+1}{r} a_t^{2'} - \frac{\psi}{r^4 f} (i\omega a_x^3 + \psi a_t^2) = 0, \quad (59)$$

$$a_x^{3''} + \left(\frac{d+z-1}{r} + \frac{f'}{f} \right) a_x^{3'} - \frac{1}{r^{2z+2} f^2} (-\omega^2 a_x^3 + i\omega \psi a_t^2 + \psi \phi a_t^1) = 0,$$

as well as two first order constraint equations

$$i\omega a_t^{1'} - \phi' a_t^2 + \phi a_t^{2'} = 0, \quad (60)$$

$$i\omega a_t^{2'} + \phi' a_t^1 - \phi a_t^{1'} + r^{2z-2} f (\psi' a_x^3 - \psi a_x^{3'}) = 0. \quad (61)$$

Obviously, a_y^3 is independent of other components, while a_x^3 mixes with a_t^1 and a_t^2 . We impose the ingoing wave conditions at the horizon

$$a_y^3(r) = (r - r_+)^{-i\omega/4\pi T} (1 + a_{y31}(r - r_+) + a_{y32}(r - r_+)^2 + a_{y33}(r - r_+)^3 + \dots), \quad (62)$$

$$a_t^1(r) = (r - r_+)^{-i\omega/4\pi T} (a_{t11}(r - r_+) + a_{t12}(r - r_+)^2 + a_{t13}(r - r_+)^3 + \dots),$$

$$a_t^2(r) = (r - r_+)^{-i\omega/4\pi T} (a_{t21}(r - r_+) + a_{t22}(r - r_+)^2 + a_{t23}(r - r_+)^3 + \dots), \quad (63)$$

$$a_x^3(r) = (r - r_+)^{-i\omega/4\pi T} (1 + a_{x31}(r - r_+) + a_{x32}(r - r_+)^2 + a_{x33}(r - r_+)^3 + \dots).$$

On the other hand, near the boundary $r \rightarrow \infty$, the expansion forms for these perturbations are listed in Tab. III. As noticed in Ref. [7], there exist two gauge freedoms for a_x^3 . To calculate the conductivity along the x direction, one can construct the gauge invariant quantity

$$\hat{a}_x^3 = a_x^3 + \psi \frac{i\omega a_t^2 + \phi a_t^1}{\phi^2 - \omega^2}. \quad (64)$$

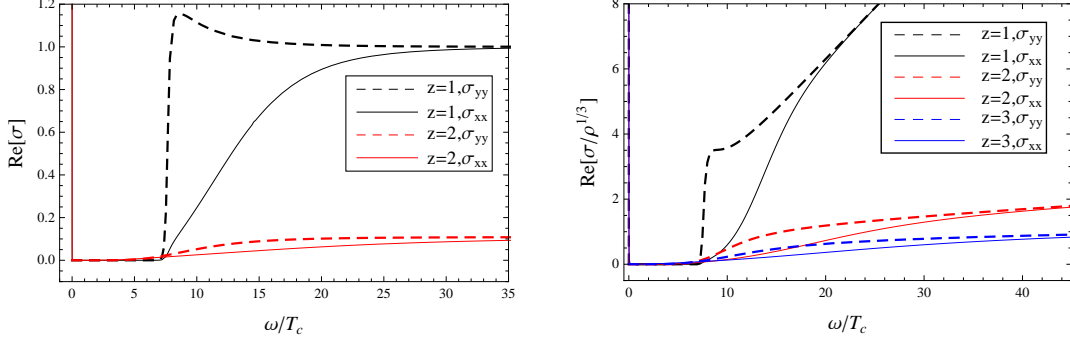


FIG. 7: The real part of the AC conductivity versus frequency of σ_{yy} (dashed) and σ_{xx} (solid) at $T/T_c \approx 0.1$ in the black hole backgrounds. The left (right) plot corresponds to the case in $D = 4$ ($D = 5$) dimensions, respectively.

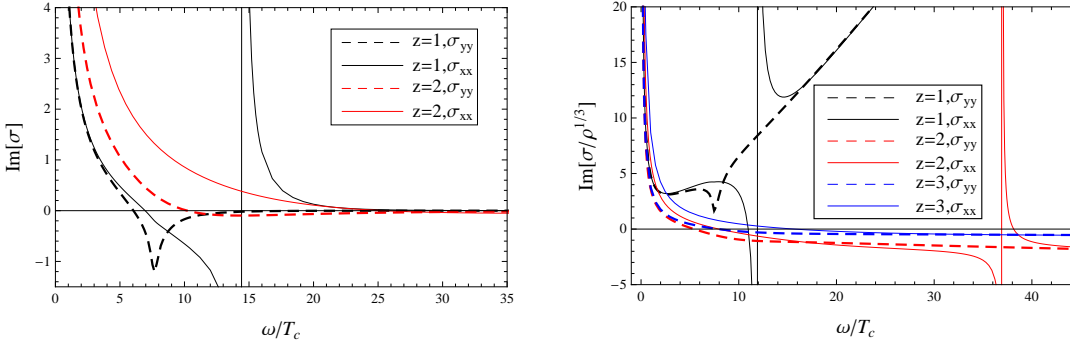


FIG. 8: The imaginary part of the AC conductivity versus frequency of a_y^3 (dashed) and a_x^3 (solid) at $T/T_c \approx 0.1$ in the 4- (left) and 5- (right) dimensional black hole backgrounds with $z = 1$ (black), 2 (red), 3 (blue).

And the conductivity can be expressed as

$$\sigma_{xx}(\omega) = \frac{\hat{a}_x^{3(1)}}{i\omega\hat{a}_x^{3(0)}}, \quad (65)$$

where $\hat{a}_x^{3(0)}$ and $\hat{a}_x^{3(1)}$ are the leading term and the coefficient of the sub-leading term of the expansion of \hat{a}_x^3 near the boundary. The conductivity along the y direction σ_{yy} is of the same form as the one in (18). Note that when a logarithmic term appears in the conductivity, it is removed by the holographic renormalization as in the case of the s-wave model. The conductivity σ_{yy} and σ_{xx} are plotted in Figs. 7 and 8.

Figure 7 exhibits the real part of the conductivity. We can see that when $z = 1$, there is an obvious energy gap from the conductivity in the y direction, as the case in the s-wave model, while the energy gap becomes not so obvious in the x direction. This is an obvious signature of the anisotropy for the p-wave superconductor model. Note that here the condensation appears in the x direction. When z increases, we can see clearly that in both cases with $D = 4$ and $D = 5$, the

TABLE IV: Some relevant quantities of the p-wave superconductor in the 4(5)-dimensional Lifshitz black hole backgrounds, where $t = 1 - T/T_c$. $\langle J_x \rangle^{1/\Delta}/\rho^{1/d}$, $n_s^y/\rho^{(d+z-2)/d}$ and $n_s^x/\rho^{(d+z-2)/d}$ are calculated near T_c . The subscript SL denotes the quantities calculated by the Sturm-Liouville variational method.

D	z	Δ	$T_c/\rho^{z/d}$	$\langle J_x \rangle^{1/\Delta}/\rho^{1/d}$	$n_s^y/\rho^{(d+z-2)/d}$	$n_s^x/\rho^{(d+z-2)/d}$	$T_{c;SL}/\rho^{z/d}$	$\langle J_x \rangle_{SL}^{1/\Delta}/\rho^{1/d}$
4	1	2	0.125	$1.40t^{1/2\Delta}$	$3.19t$	$1.04t$	0.124	1.16
4	2	3	0.037	$0.76t^{1/2\Delta}$	$0.93t$	$0.85t$	—	—
5	1	3	0.201	$1.62t^{1/2\Delta}$	$4.75t$	$2.37t$	0.199	1.37
5	2	4	0.065	$0.84t^{1/2\Delta}$	$0.91t$	$0.90t$	0.065	0.77
5	3	5	0.020	$0.65t^{1/2\Delta}$	$0.22t$	$0.36t$	—	—

conductivity is obviously suppressed in both directions. In those cases, the energy gap is also not very obvious. In addition, the difference between the conductivity along the x and y directions is also reduced as z increases. This is the effect of the anisotropic scaling of the black hole background spacetime.

Figure 8 shows the imaginary part of the conductivity. We can see from the figure that when $z = 1$ in $D = 4$ and $D = 5$, there exists an obvious minimum in the conductivity in the y direction, while in other cases, the minimum disappears. This is consistent with the observation from the real part of the conductivity that when $z = 1$, there exists an obvious energy gap along the y direction, while it disappears in other cases. In addition, when $z = 2$ in $D = 4$ and $z = 3$ in $D = 5$ there does not exist a pole at a finite frequency in the imaginary part of the conductivity along the x direction. The absence of the pole is due to the existence of the logarithmic term in the expansion of ϕ near the boundary. In fact, in this case the pole is pushed to the infinity of frequency, which can be seen from (64).

We display the superfluid density n_s^y (n_s^x) along the y (x) direction in the left plot of Fig. 9. We see that when z increases, the superfluid density decreases. This indicates that the superconductivity becomes weak as z increases, which is consistent with the behavior of the condensation. Furthermore, near the critical point, we see that n_s^y (n_s^x) behaves like $(1 - T/T_c)$ in all cases.

Now we study the behavior of the p-wave model near the transition point by the Sturm-Liouville variational method. Near the critical point, the condensation is small, thus we can assume that the $\phi(u)$ obeys the form (21), while the condensed field takes

$$\psi(u) = \frac{\langle J_x \rangle}{r_+^{d+z-2}} u^{d+z-2} F(u), \quad (66)$$

where $F = 1 - \alpha u^2$. We can recast Eq. (54) to the form of the eigenvalue problem equation (23)

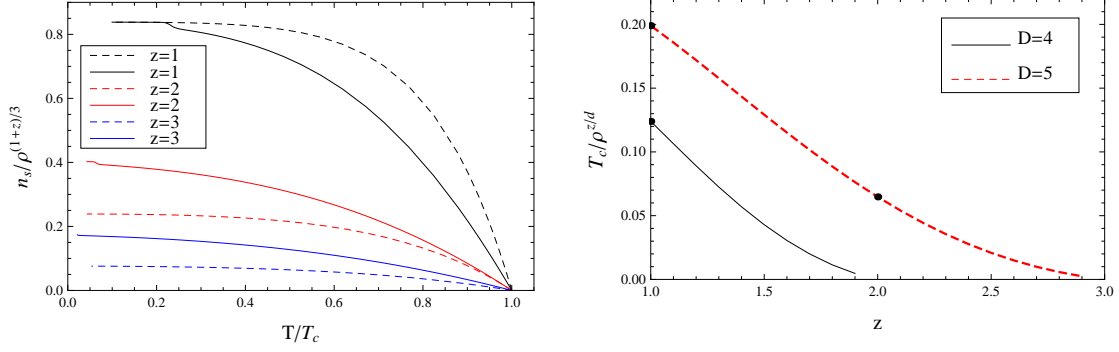


FIG. 9: The superfluid density versus temperature (left) and the critical temperature T_c versus z (right) of the p-wave model. In the left plot, the solid curves denote n_s^x , while the dashed ones mean n_s^y .

with

$$\mathcal{T} = u^{d+z-1} (1 - u^{d+z}), \mathcal{P} = (d+z)(d+z-2)u^{2d+2z-3}, \mathcal{Q} = -\frac{u^{d+z-3} (u^d - u^z)^2}{u^{d+z} - 1}. \quad (67)$$

As in the case of s-wave model, we can determine the critical temperature by the variational method. The critical temperature as a function of z is plotted in the right plot of Fig. 9. It follows that T_c decreases when z increases, which indicates that the increasing z inhibits the phase transition. This is consistent with the numerical calculation. In the same way, we can obtain the condensation behavior near the critical point. The critical temperature and condensation are listed in Tab.IV. One can see that the analytical method gives consistent results with the numerical ones.

B. p-wave superconductors in the Lifshitz soliton background

In this subsection we consider a p-wave superconductor model in the Lifshitz soliton background (33). This case corresponds to the insulator/superconductor phase transition at zero temperature. In the Lifshitz soliton background, the equations of motion of $\psi(r)$ and $\phi(r)$ turn out to be

$$\psi'' + \left(\frac{d+z-1}{r} + \frac{f'}{f} \right) \psi' + \frac{\phi^2}{r^4 f} \psi = 0, \quad (68)$$

$$\phi'' + \left(\frac{d+z-1}{r} + \frac{f'}{f} \right) \phi' - \frac{\psi^2}{r^4 f} \phi = 0, \quad (69)$$

It is interesting to note that these two equations are the same as those of the SU(2) Yang-Mills gauge field in a $(d+z+2)$ -dimensional AdS soliton background. This shows the equivalence between them in the probe approximation. Now we are going to solve these two equations. The boundary conditions of $\psi(r)$ and $\phi(r)$ at the tip $r = r_0$ are the same as those in the case of the s-wave model. On the other hand, near the boundary $r \rightarrow \infty$, the general solution of $\psi(r)$ has the

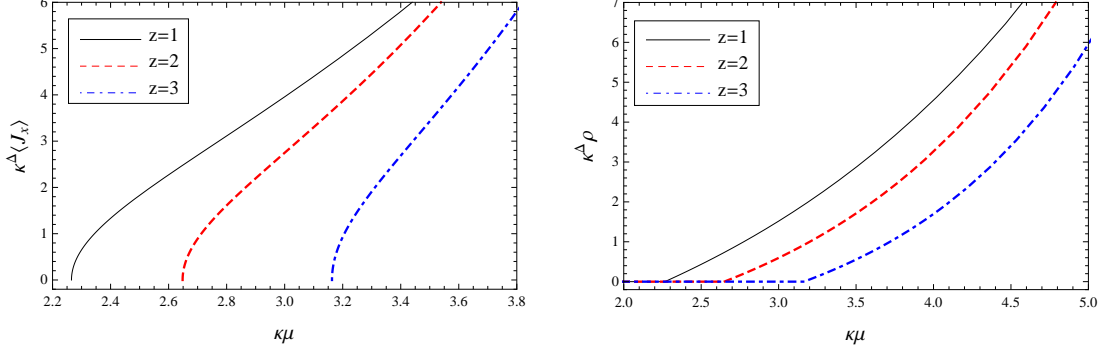


FIG. 10: The condensation (left) and the charge density (right) versus chemical potential of the p-wave model in a 5-dimensional soliton background, here $\kappa = (4/(3+z))^{1/z}$.

form (56), while $\phi(r)$ takes the form (36). We plot the condensation $\langle J_x \rangle$ and the charge density ρ in $D = 5$ in Fig. 10. It is easy to see that in this case, when z increases, the critical chemical potential increases. This implies that when z increases, the phase transition happens difficult. Near the critical point, we see that $\rho = C_\rho(\mu - \mu_c)$ and $\langle \mathcal{O} \rangle = C_{\mathcal{O}}\sqrt{\mu - \mu_c}$ in all cases. This shows, once again, the universal behavior of the critical exponent. In Tab. VI we list some results on the critical chemical potential and condensation with different z in $D = 4$ and $D = 5$ cases. Note that when $z = 1$ in $D = 5$, our results can recover the ones in Refs. [18, 21, 22].

In the presence of the condensation along the x direction, the perturbation along the x direction is expected to be mixed with other components. To calculate the conductivity along the x direction σ_{xx} , we should turn on as many components as possible and then obtain a set of self-consistent equations for the perturbation. Considering the axial gauge $A_r^a = 0$, we turn on the general perturbation in $D = 5$ as

$$\delta A = e^{-i\omega t} a_\mu^a \tau^a dx^\mu, \quad a = 1, 2, 3, \mu = t, x, y, \chi. \quad (70)$$

In the case of $D = 4$, we have to turn off a_y^a since this direction is absent in that case. The linearized Yang-Mills equations result in the equation about a_y^3 (only in $D = 5$)

$$a_y^{3''} + \left(\frac{f'}{f} + \frac{d+z-1}{r} \right) a_y^{3'} + \frac{\omega^2}{r^4 f} a_y^3 - \frac{\psi^2}{r^4 f} a_y^3 = 0, \quad (71)$$

and three equations about a_x^3 (in $D = 4, 5$)

$$\begin{aligned} a_t^{1''} + \left(\frac{f'}{f} + \frac{d+z-1}{r} \right) a_t^{1'} + \frac{\psi\phi}{r^4 f} a_x^3 &= 0, \\ a_t^{2''} + \left(\frac{f'}{f} + \frac{d+z-1}{r} \right) a_t^{2'} - \frac{\psi(a_t^2\psi + i\omega a_x^3)}{r^4 f} &= 0, \\ a_x^{3''} + \left(\frac{f'}{f} + \frac{d+z-1}{r} \right) a_x^{3'} + \frac{\omega^2 a_x^3 - i\omega a_t^2\psi - a_t^1\psi\phi}{r^4 f} &= 0, \end{aligned} \quad (72)$$

TABLE V: The asymptotical expansions of the perturbation of a_y^3 and a_x^3 in 4 (5)-dimensional soliton background, where $\mu = x, y$ in $d = 3$ and x in $d = 2$, and $i = 1, 2$.

	$d = 3(2), z = 1(2)$	$d = 3(2), z = 2(3)$	$d = 3, z = 3$	$d = 2, z = 1$
$a_t^i(r)$	$a_t^{i(0)} + \frac{a_t^{i(2)}}{r^2}$	$a_t^{i(0)} + \frac{a_t^{i(3)}}{r^3}$	$a_t^{i(0)} + \frac{a_t^{i(4)}}{r^4}$	$a_t^{i(0)} + \frac{a_t^{i(1)}}{r}$
$a_\mu^3(r)$	$a_\mu^{3(0)} + \frac{a_\mu^{3(2)}}{r^2} + \frac{a_\mu^{3(0)}\omega^2}{2r^2} \ln \xi r$	$a_\mu^{3(0)} + \frac{a_\mu^{3(0)}\omega^2}{2r^2} + \frac{a_\mu^{3(3)}}{r^3}$	$a_\mu^{3(0)} + \frac{a_\mu^{3(0)}\omega^2}{4r^2} + \frac{a_\mu^{3(4)}}{r^4} + \frac{a_\mu^{3(0)}\omega^4}{16r^4} \ln \xi r$	$a_\mu^{3(0)} + \frac{a_\mu^{3(1)}}{r}$

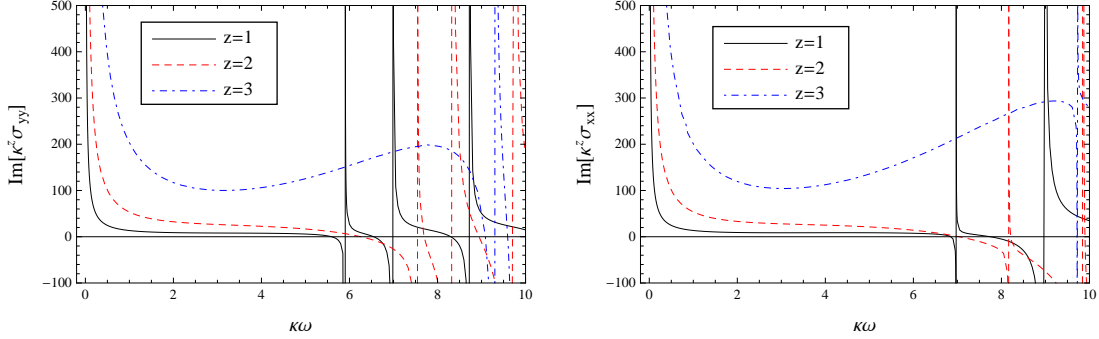


FIG. 11: The imaginary part of the conductivity versus frequency of a_y^3 (left) and a_x^3 (right) at $\mu/\mu_c \approx 4$ in the 5-dimensional soliton background with $z = 1, 2, 3$, here $\kappa = (4/(3+z))^{1/z}$.

as well as two constraint equations

$$i\omega a_t^{1'} - \phi' a_t^2 + \phi a_t^{2'} = 0, \quad (73)$$

$$i\omega a_t^{2'} + \phi' a_t^1 - \phi a_t^{1'} + \psi' a_x^3 - \psi a_x^{3'} = 0. \quad (74)$$

The other components decouple from a_y^3 , a_t^1 , a_t^2 and a_x^3 . The boundary conditions of the above components at the tip are similar to those in (38), while near the boundary $r \rightarrow \infty$, the general falloffs are listed in Tab. V.

In Fig. 11 we plot the imaginary part of the conductivity along the y direction (left plot) and the x direction (right plot) for the p-wave model in $D = 5$, while we list the superfluid density n_s^y (n_s^x) associated with σ_{yy} (σ_{xx}) in Tab. VI, from which we have the following observations. Along the y and x directions, the position of the second pole in the imaginary part of the conductivity moves toward the right as z increases, which means that the energy of the quasiparticle excitation increases as we increase z . What is more, the frequency ω_s^x of the second pole in the x direction is larger than ω_s^y in the y direction in $D = 5$. This indicates that to have a quasi-particle excitation along the x direction (the condensing direction), one has to pay more energy than in the y direction. In addition, we see that the difference between ω_s^x and ω_s^y decreases when z increases, which indicates that the anisotropy of the conductivity is suppressed with the increasing z .

As in the s-wave model, we can also obtain a Sturm-Liouville eigenvalue equation (41) for the

TABLE VI: Some quantities of the p-wave model in $D = 4$ (5), where $t = (\mu/\mu_c - 1)^{1/2}$ and quantities $\langle J_x \rangle$, $\langle J_x \rangle_{SL}$, ρ , ρ_{SL} , n_s^x and n_s^y are all calculated near μ_c . Here, $\kappa = (4/(d+z))^{1/z}$ and the subscript SL denotes the quantity calculated by the Sturm-Liouville variational method.

D	z	$\kappa\mu_c$	$\kappa^\Delta \langle J_x \rangle$	$\kappa^{d+z-1} \rho$	$\kappa^{d+z-2} n_s^y$	$\kappa \omega_s^y$	$\kappa^{d+z-2} n_s^x$	$\kappa \omega_s^x$	$\kappa \mu_{c;SL}$	$\kappa^\Delta \langle J_x \rangle_{SL}$	$\kappa^{d+z-1} \rho_{SL}$
4	1	1.988	$4.12t$	$3.71t^2$	–	–	$1.86t^2$	6.61	1.988	$2.24t$	$2.07t^2$
4	2	2.265	$5.19t$	$3.98t^2$	–	–	$3.54t^2$	6.98	2.267	$3.85t$	$2.56t^2$
4	3	2.749	$7.18t$	$4.66t^2$	–	–	$5.01t^2$	8.50	2.752	$6.19t$	$3.36t^2$
5	1	2.265	$5.19t$	$3.99t^2$	$3.54t^2$	5.90	$3.54t^2$	6.97	2.267	$3.85t$	$2.56t^2$
5	2	2.648	$6.18t$	$4.01t^2$	$4.07t^2$	7.54	$4.07t^2$	8.17	2.652	$6.07t$	$3.24t^2$
5	3	3.163	$8.38t$	$4.59t^2$	$5.79t^2$	9.32	$5.80t^2$	9.32	3.171	$9.12t$	$4.19t^2$

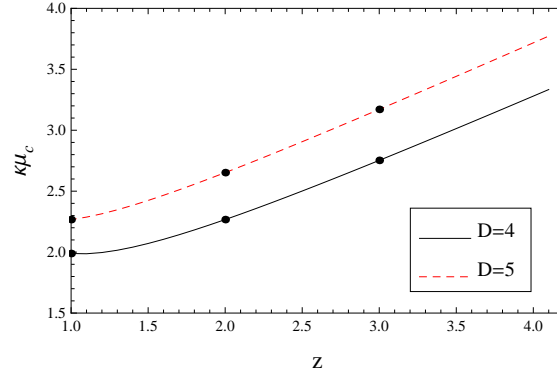


FIG. 12: The critical chemical potential μ_c with respect to z of the p-wave models in the Lifshitz soliton background, here $\kappa = (4/(d+z))^{1/z}$.

p-wave model in $D = 5$ with

$$\mathcal{T} = u^{z+2} (1 - u^{z+3}), \quad \mathcal{P} = (z^2 + 4z + 3) u^{2z+3}, \quad \mathcal{Q} = u^{z+2}. \quad (75)$$

Solving the equation, we can determine the critical chemical potential with arbitrary $z \geq 1$, which is plotted in Fig. 12. The case of $D = 4$ can be done in a similar way. One can find that the critical chemical potential μ_c increases with the increase of z . This is consistent with the numerical calculation. Furthermore we list the critical chemical potential, condensation and charge density in Tab. VI from the analytical method, for a comparison with the numerical calculation. Once again, both methods show agreement results. This shows that the analytical method is indeed powerful and universal. Finally we mention here that when $z = 1$ and $D = 5$, our results can recover those in Refs. [17, 19, 21].

IV. CONCLUSIONS AND DISCUSSIONS

In this paper, by numerical and analytical methods we have studied the properties of the holographic superconductor models in 4- and 5-dimensional Lifshitz black hole and soliton spacetimes, respectively. These models correspond to the conductor/superconductor and insulator/superconductor phase transitions in condensed matter physics. We have discussed the s-wave and p-wave models by introducing a complex scalar field and SU(2) gauge field in the bulk, respectively. We have emphasized the influence of the dynamical critical exponent z on the properties of the holographic superconductor models. Main conclusions can be summarized as follows.

- (1) In the case with the Lifshitz black hole background, for both the s-wave and p-wave models, when z increases, the critical temperature decreases, which suggests that the phase transition becomes hard as z increases. When z increases, the conductivity is suppressed in both the s-wave and p-wave cases; the difference between the conductivity along the different directions, σ_{yy} and σ_{xx} , decreases in the p-wave case. This indicates that when z increases, the anisotropic effect in the p-wave model becomes weak. The superfluid density decreases as z increases, which is consistent with the behavior of the conductivity. But, we observed that near the critical point, the condensation always behaves as $\sim (1 - T/T_c)^{1/2}$ in the case with a general z and D . This shows that the critical exponent is universal, consistent with the result from the mean field theory.
- (2) In the case with the Lifshitz soliton background, when z increases, the critical chemical potential μ_c decreases in the s-wave models but increases in the p-wave cases. This result looks strange, but it can be understood by noting the fact that in the s-wave case, we fix the dimension of the scalar operator, while in the p-wave case, the mass of the vector field is fixed (in fact, the effective mass of the vector field is zero). In Fig. 13 we plot the critical chemical potential μ_c with various z and mass the scalar field in the s-wave model. We can see clearly that for a fixed mass, the critical chemical potential increases when z increases, which is in agreement with the case of the p-wave model. In the p-wave model, we have found that the difference between σ_{xx} and σ_{yy} decreases with the increase of z , which implies that the increasing z suppresses the anisotropy of the p-wave superconductor. In addition, near the critical point, the condensation always behaves as $\sim (\mu - \mu_c)^{1/2}$ in all cases. Once again, this shows the universality of the critical exponent.
- (3) In both the cases with the black hole and soliton backgrounds, by employing the Sturm-

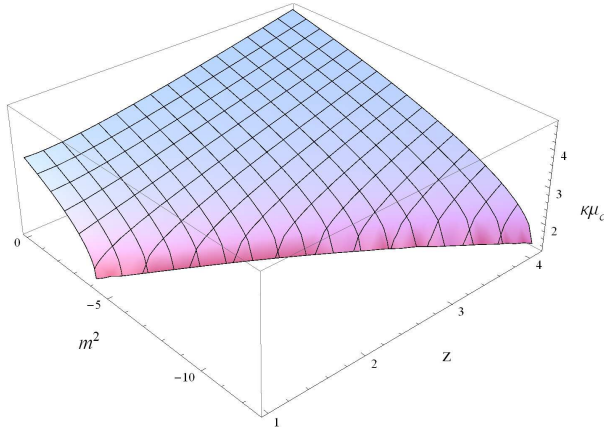


FIG. 13: The critical chemical potential μ_c versus z and m^2 of the s-wave models in the 5 dimensional solitons.

Liouville variational method, we have studied the behavior of these holographic superconductor models near the critical point, and obtained consistent results as in the numerical calculation. This shows that the variational method is quite useful and powerful.

In a word, we have seen that when the dynamical critical exponent z increases, the superconducting phase transition becomes difficult, the superconductivity becomes weak and in the p-wave case the anisotropy is suppressed. In addition, we have found that in the $(d + 2)$ -dimensional Lifshitz soliton background, the reduced equations of motion in both the s-wave and p-wave models are the same as those in a $(d + 2 + z)$ -dimensional AdS soliton background. As a result, the superconductor models with the $(d + 2)$ -dimensional Lifshitz soliton background are equivalent to those in a $(d + 2 + z)$ -dimensional AdS soliton background. Of course, this holds only in the probe approximation.

In this paper we have only worked on the probe limit by neglecting the back reaction of the matter fields. Although the probe limit can reveal some significant properties of holographic superconductor model, it has been shown that new phases can emerge (see Refs. [34, 35] for example) and the order of the phase transition can be also changed [36, 37] once taking the back reaction into consideration. Therefore, it is interesting to study the influence of the back reaction of the matter field to the Lifshitz background and to see whether there are some new features beyond the probe limit.

Acknowledgments

We would like to thank S. A. Hartnoll for his help about the numerical code. One of the authors (J. W. Lu) is deeply grateful to R. G. Cai, Y. Y. Bu, L. Li, and M. L. Liu for their helpful discussions and comments. This work is supported by the National Natural Science Foundation of China (Grant No. 11175077), the Natural Science Foundation of Liaoning Province (Grant No. L2011189) and the PhD Programs of Ministry of China (Grant No. 20122136110002).

-
- [1] J. M. Maldacena, “The Large N limit of superconformal field theories and supergravity,” *Adv. Theor. Math. Phys.* **2**, 231 (1998) [hep-th/9711200].
 - [2] S. S. Gubser, I. R. Klebanov and A. M. Polyakov, “Gauge theory correlators from noncritical string theory,” *Phys. Lett. B* **428**, 105 (1998) [hep-th/9802109].
 - [3] E. Witten, “Anti-de Sitter space and holography,” *Adv. Theor. Math. Phys.* **2**, 253 (1998) [hep-th/9802150].
 - [4] S. A. Hartnoll, C. P. Herzog and G. T. Horowitz, “Building a Holographic Superconductor,” *Phys. Rev. Lett.* **101**, 031601 (2008) [arXiv:0803.3295 [hep-th]].
 - [5] G. T. Horowitz and M. M. Roberts, “Holographic Superconductors with Various Condensates,” *Phys. Rev. D* **78**, 126008 (2008) [arXiv:0810.1077 [hep-th]].
 - [6] G. Siopsis and J. Therrien, “Analytic Calculation of Properties of Holographic Superconductors,” *JHEP* **1005**, 013 (2010) [arXiv:1003.4275 [hep-th]].
 - [7] S. S. Gubser and S. S. Pufu, “The Gravity dual of a p-wave superconductor,” *JHEP* **0811**, 033 (2008) [arXiv:0805.2960 [hep-th]].
 - [8] F. Aprile, D. Rodriguez-Gomez and J. G. Russo, “p-wave Holographic Superconductors and five-dimensional gauged Supergravity,” *JHEP* **1101**, 056 (2011) [arXiv:1011.2172 [hep-th]].
 - [9] R. -G. Cai, Z. -Y. Nie and H. -Q. Zhang, “Holographic p-wave superconductors from Gauss-Bonnet gravity,” *Phys. Rev. D* **82**, 066007 (2010) [arXiv:1007.3321 [hep-th]].
 - [10] R. -G. Cai, Z. -Y. Nie and H. -Q. Zhang, “Holographic Phase Transitions of P-wave Superconductors in Gauss-Bonnet Gravity with Back-reaction,” *Phys. Rev. D* **83**, 066013 (2011) [arXiv:1012.5559 [hep-th]].
 - [11] R. -G. Cai, S. He, L. Li and L. -F. Li, “A Holographic Study on Vector Condensate Induced by a Magnetic Field,” arXiv:1309.2098 [hep-th].
 - [12] R. -G. Cai, L. Li and L. -F. Li, “A Holographic P-wave Superconductor Model,” arXiv:1309.4877 [hep-th].
 - [13] J. -W. Chen, Y. -J. Kao, D. Maity, W. -Y. Wen and C. -P. Yeh, “Towards A Holographic Model of D-Wave Superconductors,” *Phys. Rev. D* **81**, 106008 (2010) [arXiv:1003.2991 [hep-th]].
 - [14] F. Benini, C. P. Herzog, R. Rahman and A. Yarom, “Gauge gravity duality for d-wave superconductors:

- prospects and challenges,” *JHEP* **1011**, 137 (2010) [arXiv:1007.1981 [hep-th]].
- [15] K. -Y. Kim and M. Taylor, “Holographic d-wave superconductors,” *JHEP* **1308**, 112 (2013) [arXiv:1304.6729 [hep-th]].
- [16] T. Nishioka, S. Ryu and T. Takayanagi, “Holographic Superconductor/Insulator Transition at Zero Temperature,” *JHEP* **1003**, 131 (2010) [arXiv:0911.0962 [hep-th]].
- [17] H. -F. Li, “Further studies on holographic insulator/superconductor phase transitions from Sturm-Liouville eigenvalue problems,” *JHEP* **1307**, 135 (2013) [arXiv:1306.3071 [hep-th]].
- [18] R. -G. Cai, X. He, H. -F. Li and H. -Q. Zhang, “Phase transitions in AdS soliton spacetime through marginally stable modes,” *Phys. Rev. D* **84**, 046001 (2011) [arXiv:1105.5000 [hep-th]].
- [19] R. -G. Cai, H. -F. Li and H. -Q. Zhang, “Analytical Studies on Holographic Insulator/Superconductor Phase Transitions,” *Phys. Rev. D* **83**, 126007 (2011) [arXiv:1103.5568 [hep-th]].
- [20] Q. Pan, J. Jing and B. Wang, “Analytical investigation of the phase transition between holographic insulator and superconductor in Gauss-Bonnet gravity,” *JHEP* **1111**, 088 (2011) [arXiv:1105.6153 [gr-qc]].
- [21] A. Akhavan and M. Alishahiha, “P-Wave Holographic Insulator/Superconductor Phase Transition,” *Phys. Rev. D* **83**, 086003 (2011) [arXiv:1011.6158 [hep-th]].
- [22] R. -G. Cai, L. Li, L. -F. Li and R. -K. Su, “Entanglement Entropy in Holographic P-Wave Superconductor/Insulator Model,” *JHEP* **1306**, 063 (2013) [arXiv:1303.4828 [hep-th]].
- [23] C. O. Lee, “The holographic superconductors in higher-dimensional AdS soliton,” *Eur. Phys. J. C* **72**, 2092 (2012) [arXiv:1202.5146 [gr-qc]].
- [24] S. Kachru, X. Liu and M. Mulligan, “Gravity Duals of Lifshitz-like Fixed Points,” *Phys. Rev. D* **78**, 106005 (2008) [arXiv:0808.1725 [hep-th]].
- [25] M. Taylor, “Non-relativistic holography,” arXiv:0812.0530 [hep-th].
- [26] D. -W. Pang, “A Note on Black Holes in Asymptotically Lifshitz Spacetime,” arXiv:0905.2678 [hep-th].
- [27] E. J. Brynjolfsson, U. H. Danielsson, L. Thorlacius and T. Zingg, “Holographic Superconductors with Lifshitz Scaling,” *J. Phys. A* **43**, 065401 (2010) [arXiv:0908.2611 [hep-th]].
- [28] S. -J. Sin, S. -S. Xu and Y. Zhou, “Holographic Superconductor for a Lifshitz fixed point,” *Int. J. Mod. Phys. A* **26**, 4617 (2011) [arXiv:0909.4857 [hep-th]].
- [29] Y. Bu, “Holographic superconductors with $z = 2$ Lifshitz scaling,” *Phys. Rev. D* **86**, 046007 (2012) [arXiv:1211.0037 [hep-th]].
- [30] Z. Fan, “Holographic superconductors with hyperscaling violation,” *JHEP* **1309**, 048 (2013) [arXiv:1305.2000 [hep-th]].
- [31] E. Abdalla, J. de Oliveira, A. B. Pavan and C. E. Pellicer, “Holographic phase transition and conductivity in three dimensional Lifshitz black hole,” arXiv:1307.1460 [hep-th].
- [32] R. -G. Cai and H. -Q. Zhang, “Holographic Superconductors with Horava-Lifshitz Black Holes,” *Phys. Rev. D* **81**, 066003 (2010) [arXiv:0911.4867 [hep-th]].
- [33] S. A. Hartnoll and R. Pourhasan, “Entropy balance in holographic superconductors,” *JHEP* **1207**, 114

- (2012) [arXiv:1205.1536 [hep-th]].
- [34] R. -G. Cai, L. Li, L. -F. Li and Y. -Q. Wang, “Competition and Coexistence of Order Parameters in Holographic Multi-Band Superconductors,” JHEP **1309**, 074 (2013) [arXiv:1307.2768 [hep-th]].
- [35] Y. Liu, K. Schalm, Y. -W. Sun and J. Zaanen, “Bose-Fermi competition in holographic metals,” JHEP **1310**, 064 (2013) [arXiv:1307.4572 [hep-th]].
- [36] G. T. Horowitz and B. Way, “Complete Phase Diagrams for a Holographic Superconductor/Insulator System,” JHEP **1011**, 011 (2010) [arXiv:1007.3714 [hep-th]].
- [37] R. -G. Cai, S. He, L. Li and L. -F. Li, “Entanglement Entropy and Wilson Loop in Stúckelberg Holographic Insulator/Superconductor Model,” JHEP **1210**, 107 (2012) [arXiv:1209.1019 [hep-th]].